© 2024 Optica Publishing Group. One print or electronic copy may be made for personal use only. Systematic reproduction and distribution, duplication of any material in this paper for a fee or for commercial purposes, or modifications of the content of this paper are prohibited.

link to online abstract
https://doi.org/10.1364/oe.519995

Research Article Vol. 32, No. 14 / 1 Jul 2024 / Optics Express 24553

Optics EXPRESS

High throughput compressive fluorescence lifetime imaging with a silicon photomultiplier detector

ALBERTO GHEZZI,[1,2] ELISABETTA AVANZI,[1] ARIEL GARCÍA FLEITAS,[1,3] LAURA DI SIENO,[1] ALBERTO DALLA MORA,[1] STEFANO SANTABARBARA,[4] ANDREA BASSI,[1,2] GIANLUCA VALENTINI,[1,2] ANDREA FARINA,[2,*] AND COSIMO D'ANDREA[1,3]

[1] *Politecnico di Milano, Dipartimento di Fisica, Piazza L. da Vinci 32, 20133 Milano, Italy*
[2] *Consiglio Nazionale delle Ricerche, Istituto di Fotonica e Nanotecnologie, Piazza L. da Vinci 32, 20133 Milano, Italy*
[3] *Istituto Italiano di Tecnologia, Center for Nano Science and Technology, Via Raffaele Rubattino, 81, 20134 Milano, Italy*
[4] *Istituto di Biologia e Biotecnologia Agraria, Consiglio Nazionale Delle Ricerche, Via Bassini 15a, 20133, Milan, Italy*
[*] *andrea.farina@cnr.it*

Abstract: Fluorescence lifetime imaging microscopy (FLIM) is a powerful technique for studying biological processes. There exists a growing interest in developing strategies to enhance throughput and reduce acquisition time of FLIM systems, which commonly employ laser scanning excitation and time-correlated single-photon counting (TCSPC) detection. In this work, we propose a wide-field FLIM microscope based on compressive sensing and high photon rate detection (beyond pile-up limit) based on a high-efficiency silicon photomultiplier detector as a single-pixel camera. We experimentally validate the capabilities of this design achieving 20 frames per second FLIM images on free-moving green algae sample.

© 2024 Optica Publishing Group under the terms of the Optica Open Access Publishing Agreement

1. Introduction

Fluorescence lifetime, i.e., the average time a fluorophore stays in the excited state, is a fundamental physical property for studying the interactions between a fluorophore and its local microenvironment. In fact, the analysis of the fluorescence lifetime of a fluorophore and its variation can provide clues on pH, ion concentration and any molecular interactions undergone by the fluorophore [1]. In particular, fluorescence lifetime imaging microscopy (FLIM) has relevant applications in life sciences, e.g., to study intracellular activities or metabolic states [2]. Biological samples are intrinsically dynamic systems due to their movement and physiological changes, which can cause rapid variations of the fluorescence properties of endogenous or exogenous fluorochromes. Hence, there exists a growing interest for advancing fast FLIM acquisition methods [3,4].

A common way to measure the fluorescence lifetime is through the time-correlated single-photon counting (TCSPC) technique: the sample is excited with high-repetition-rate laser pulses, which are scanned across the field of view (FOV). For any laser pulse, a single fluorescence photon, among those emitted during the excitation cycle, is classified in a temporal scale and counted to construct a histogram of the photon distribution over time.

In TCSPC-FLIM, the counting process continues until a sufficient number of photons is collected to allow the lifetime estimation [5], e.g., by an exponential model fitting. Although this can be faster achieved by increasing the excitation power density (i.e., with higher photon

#519995 https://doi.org/10.1364/OE.519995
Journal © 2024 Received 6 Feb 2024; revised 12 May 2024; accepted 20 May 2024; published 21 Jun 2024

Optics EXPRESS

rate), this is often not an option due to the low photostability of biologic samples, which must be measured under low illumination power densities. Hence, most of the research effort has been devoted to increasing photon collection and detection efficiency. Moreover, TCSPC systems suffer from an associated instrumental dead time (ranging from tens to hundreds of nanoseconds) required for assigning the proper timing to each detected photon and to restore the operative conditions. Photons arriving within dead time are lost. Hence, fast TCSPC-FLIM systems are often developed by using time-to-digital converters (TDCs) featuring a low dead time [6]. At the same time, the maximum count rate in TCSPC-FLIM measurements must typically be maintained below 5% [7] of the excitation rate to avoid distortion effects (pile-up) in the time-resolved fluorescence histogram [1] and, for this reason, the photon rate is typically limited or possibly split into different detection channels working in parallel [8].

On the one hand, acousto-optical deflectors, for acquiring only in limited region of interests (ROI) [9], fast resonance scanners, or multi-beam scanning systems coupled to multichannel detector arrays [10] have been considered to increase the acquisition speed. On the other hand, the highest imaging speed can be attained using wide field schemes rather than scanning ones. The state-of-the-art implementations rely on time-gated intensified cameras, but these have lower time resolutions than TCSPC systems [8]. Recently, wide-field FLIM systems with arrays of single-photon avalanche diodes (SPADs) featuring a TDC for each pixel have been presented [11,12]. These schemes, indeed promising, have to cope with an increased system complexity, broad instrumental response function (hundreds of picoseconds) and fill factor limitations (28%, up to 42% by adopting microlenses) [8].

Another strategy for increasing the throughput of TCSPC-FLIM systems is based on computational imaging, a method which requires a computational step to obtain the image. In particular, compressive sensing (CS) combined with single-pixel camera (SPC) [13] is a computational imaging technique that combines the speed of a wide-field acquisition, by means of spatial light modulators, with the benefits of a high performance detector with a single active element [14]. By exploiting CS methods, it is possible to obtain an image with N pixels from $M < N$ measurements, without relevant loss of information, due to some redundancy that is intrinsic in any image. With an optimized scheme, CS methods can lead to a large reduction in acquisition time. Computational imaging based on CS and spatial light modulators is emerging as a promising framework for high throughput FLIM systems [15].

In our recent work [16], a system for computational wide-field FLIM based on the single-pixel camera acquisition scheme has been presented. The system requires the sample to be illuminated by a collection of pseudo-random binary patterns. The fluorescence related to each pattern is integrated by a lens to a single-pixel detector. Then, a computation is performed for image reconstruction. We showed the capability of this scheme to reduce the number of necessary measurements by 70% compared to a conventional scanning scheme, allowing us to obtain a multispectral FLIM image in 3 seconds. However, the system was limited by the maximum photon count rate (1 million counts per second, Mcps) posed by the detector and the pile-up limitation, which hindered the possibility to further increase speed without sacrificing data quality. In fact, SPC is a wide-field measurement scheme and the 1 Mcps limit can be easily reached. Nevertheless, the use of a single-pixel detector decreases the system complexity and costs since engineering a single detector for high-performance is easier than a pixelated array [17]. This paves the way to the exploitation of novel detectors, such as silicon photomultipliers (SiPMs) [6,18], which allow reduced acquisition time and highly compact detection systems, compared to those based on photomultiplier tubes (PMTs) [19]. In particular, a SiPM exhibits numerous advantages for TCSPC applications, including a 60 ps single-photon time resolution, high detection efficiency (~30% at 600 nm), high throughput (tens of Mcps), a wide collection area (a few square mm, compared to the ≈100 μm diameter of current SPADs) and scalability into arrays.

Optics EXPRESS

In this work, we propose and experimentally validate a system for high throughput TCSPC-FLIM based on compressive single-pixel camera scheme with a SiPM detector. This, in combination with CS, enables wide-field FLIM at video rates (20 frames per second, fps).

2. Materials and methods

The experimental setup is schematized in Fig. 1. The sample's fluorescence is excited with pulses from a 40 MHz mode-locked supercontinuum fiber laser (SC-450, Fianium). The laser light is filtered at 630 nm (10 nm full width at half maximum), expanded by a lens (L1, f = 25 mm), and projected onto a digital micromirror device (DMD, V-7000 ViaLUX GmbH) which is employed as a binary spatial light modulator. This device illuminates the sample with several pseudo-random patterns, as required for SPC, which are preloaded onto the device's memory. To prevent dead times in illumination, the DMD is set to project without any dark phase between consecutive patterns (uninterrupted mode). The DMD and the sample plane are optically conjugated by a 200 mm achromatic lens (L2) and a 40x objective (Plan N 40× NA 0.65 infinity corrected, Olympus Corp.). The FOV, 150×150 μm^2 wide, is illuminated with 140 μW. A dichroic mirror (DM, DMLP650R, Thorlabs, Inc.) separates the illumination light from fluorescence. The latter is then further long pass filtered (F1, FELH0650, Thorlabs, Inc.) and directed towards a cooled CMOS camera (ORCA-Flash4.0 V3, Hamamatsu Photonics K.K.) and a SiPM detector by means of a 50/50 beam splitter (BS033, Thorlabs Inc.). The sample is imaged onto the camera sensor by a tube lens made by a 200 mm achromatic doublet (L4). The fluorescence is also focused onto the single-pixel detector by a 50 mm lens and a 20x microscope objective (Plan N 20× NA 0.4 infinity corrected, Olympus Corp.). The detector is a compact ($5 \times 4 \times 9$ cm^3) SiPM based single-photon detection module (upgraded from [20]) with 1.3×1.3 mm^2 (74% fill factor) of active area, embedding a Peltier cooling stage to reduce the dark count rate. Its dead time (i.e., the shortest time between two consecutive photon detections) is less than 4 ns.

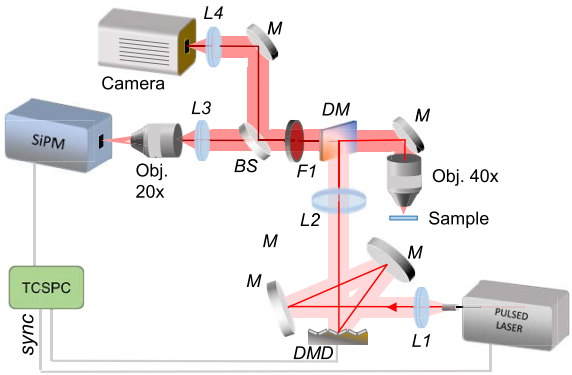

Fig. 1. Optical scheme of the experimental system. DMD: digital micromirror device, M: mirror, DM: dichroic mirror, F: filter, L: lens, Obj: objective, BS: beam splitter, TCSPC: time-correlated single-photon counting device.

The signal is then acquired using one channel of a MultiHarp 150 16P (PicoQuant GmbH), which has a minimum dead time of 650 ps, operating in time-tagging mode. The short dead time of both SiPM module and TCSPC electronics allows us to reach the limit of 40 Mcps set by the laser repetition rate. Once the acquisition is completed, the histogram representing the fluorescence decay can be retrieved from the time-tagged photon events and the sync from the laser. Moreover, when the projection of a pattern starts, a proper event is recorded in the time-tagged stream by means of a digital signal generated by the DMD to the control port of the MultiHarp 150 16P. The projection of each pattern lasts for 195 μs and each measurement

Optics EXPRESS

is performed with M = 256 patterns, to acquire an image with N = 32 × 32 pixels. Hence, a dataset is measured with a compression ratio (CR = 1-M/N) of 75%. This leads to an SPC image every 50 ms, i.e., to a frame rate of 20 fps in case of continuous measurements. The CMOS camera acquires in parallel with SPC with an exposure time of 50 ms per frame and operates in free-running mode. The acquired data is processed with in-house software written in MATLAB language [21].

The combination of an efficient detector and a high performance acquisition board enables photon counting with high throughput on a single TCSPC channel. In order not to nullify this benefit by attenuating the signal, a post-processing algorithm is applied to the acquired fluorescence decays to correct the distortion due to pile-up [22,23], before any other processing. To apply the correction, it is necessary to relate the number of photons collected in the i-th time bin (N_i) of the histogram of the photon distribution over time to the true probability of detecting, in one laser cycle, a single photon at that time bin (S_i), considering that more than one photon can be detected, but only the first one can be processed by the electronics, thus losing all the others events up to the end of the dead-time. To do so, the total number K of measurements cycles must be used. In particular [22]:

$$S_i = -\ln(1 - P_i),$$

where P_i is the probability of an event occurring in the i-th channel in one cycle, and is derived from:

$$P_i = \frac{N_i}{K - \sum_{j=1}^{i-1} N_j}.$$

Thus, the corrected number of counts in the i-th channel can be then computed as $N_i = KS_i$. Even though these equations are simple and easily implementable, they do not necessitate any assumptions regarding prior knowledge of the intrinsic shape of the curve's corrected form, nor do they require assumptions regarding the regularity or uniformity of channel widths [22]. Thanks to the short dead time of both the SiPM and the TCSPC channel, it is even possible to count more than a single event per laser pulse. For the correction algorithm to work properly, the count rate of the acquisition must be kept below the laser repetition rate (40 MHz). Moreover, the dead time of the MultiHarp 150 16P has been increased to 10 ns to prevent the detection chain from recovering in the same laser pulse, which would have produced a distortion of the signal in a way not correctable with the mentioned algorithm. To demonstrate the capability of the algorithm, we acquired fluorescence decays from a sample of fluorescent beads for different photon rates up to 35 Mcps as shown in Fig. 2(a). The decays are gradually affected by pile-up distortion, resulting in an equivalent decrease in lifetime value from 3.71 ns (at 1 Mcps) to 1.82 ns (at 35 Mcps), estimated using a bi-exponential fit. Similarly, the same decays after computational correction are shown in Fig. 2(b), all corresponding to a lifetime of 3.71 ns.

Then, the time-resolved images are reconstructed, from SPC measurements, using a CS algorithm (i.e., TVAL3, which exploits the sparsity in the gradient domain through the total variation minimization, with a toolbox developed for MATLAB, available at Ref. [24]). Finally, the fluorescence lifetime is retrieved, through maximum likelihood estimation (MLE), in all the pixels with an amplitude greater than a threshold (to avoid analysis in empty pixels). MLE is more appropriate than least squares curve fitting in case of data affected by Poisson noise and with low SNRs (as typical of fast measurements), providing more accurate estimates of lifetime values [1].

Optics EXPRESS

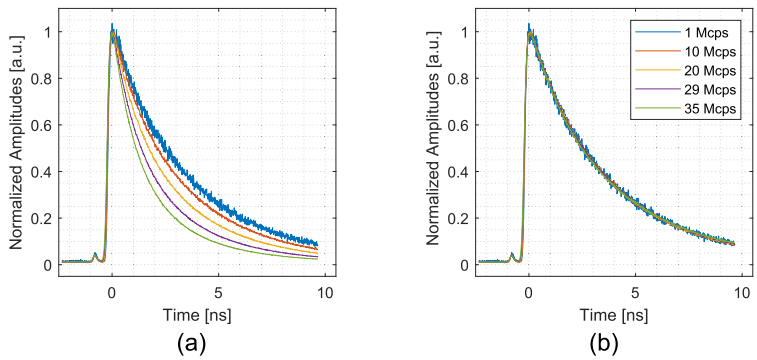

Fig. 2. (a) Raw data acquired on a fluorescent beads sample at different count rates; (b) Same data as (a) after pile-up correction, at different count rates. All curves are normalized to the peak.

3. Results and discussion

3.1. Beads sample

A microscope slide containing fluorescent beads (4 µm diameter, FocalCheck F36909, Invitrogen) was measured for validating the system performances. We firstly carried out the acquisition of 700 time-resolved SPC datasets (35 s of total measurement time) on a static FOV which are used to characterize the system's capabilities. Once image reconstruction and lifetime estimation for each dataset were carried out, the stack of 700 FLIM maps was arranged as frames of a movie, as shown in Visualization 1. The image quality of the SPC dataset has been evaluated by adopting the peak signal-to-noise ratio (PSNR) estimator [16] (PSNR = $10\log(d^2/\text{MSE})$, d is the dynamic range of the images, MSE is the mean squared error between a compressed image and a reference one), which is a standard parameter to evaluate the image quality at different levels of compression. PSNR is calculated with respect to 700 reference images acquired in parallel with the CMOS camera. The PSNR results in 22.1 ± 0.3 dB across all images. Since all the frames are acquired under equal conditions, the dispersion of the PSNR values represents an estimation of the measurement repeatability. This dispersion can be mainly attributed to the Poisson noise affecting the total number of photons of each SPC repetition.

Similarly, we selected a pixel in correspondence of a group of beads (indicated by a red arrow in Visualization 1), containing ≈ 200 counts per frame, and we evaluated the accuracy of a mono-exponential lifetime estimation, resulting in 3.10 ± 0.14 ns on average in all frames.

Then, we manually moved the sample holder in order to translate the beads across the illuminated area. The count rate within the different acquisitions is always below the laser repetition rate. The recorded SPC-FLIM frames were arranged as a movie, as shown in Visualization 2. Similarly, we evaluated the PSNR at each frame with respect to the CMOS camera images and results in 22.4 ± 1.2 dB. The PSNR value indicates a good agreement between the two imaging systems, as can be also inferred visually. The dispersion in PSNR values is higher than in the static case, as a consequence of the motion of the sample. Similarly, we selected a 3×3-pixels region of interest containing a group of beads (highlighted with a white square in Fig. 3(a), lower row) and we monitored the estimated lifetimes within the first 16 measurements, i.e., when the sample was kept still, resulting 2.92 ± 0.10 ns. Then, we monitored the same group of beads when the sample was moved (in the following 89 frames), and the estimated lifetime is 2.88 ± 0.16 ns. The similarity between PSNRs and lifetimes with static and moving sample represents an indicator that the motion did not produce significant estimation artifacts. Figure 3 shows three selected

Optics EXPRESS

frames at different positions of the beads, respectively (a) after 3.65 s, (b) 8 s and (c) 14 s from the measurement start, for both the CMOS camera (upper row) and SPC-FLIM (lower row).

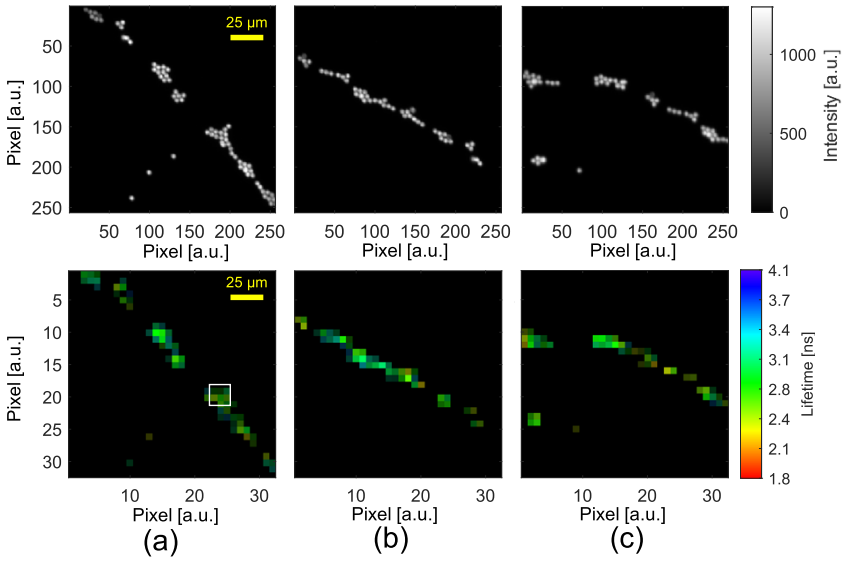

Fig. 3. Measurements with a moving beads sample at different time instants after the start of the acquisition. Upper row: reference intensity images with a high-resolution CMOS camera. Lower row: FLIM maps acquired with a CS-SPC. (a) after 3.65 s (b) after 8 s (c) after 14 s.

3.2. Green algae sample

Finally, we measured the fluorescence of the chlorophyll from moving green algae *Chlamydomonas reinhardtii*. *C. reinhardtii* has two flagella and a phototaxis apparatus and can swim towards optimal light condition. The *Chlamydomonas* strain used for the measurements is WT (CC124 mt-); it was grown in medium light (30 µE m^{-2} s^{-1}) [25,26] and under heterotrophic conditions in Tris-acetate-phosphate medium (TAP) medium that contains acetate as reduced carbon source [25]. The specimen was maintained under light and agitation before the measurements, to avoid to onset of anaerobiosis. Then, a drop was deposited on a microscope slide and the sample was kept in the dark for a few minutes before the FLIM acquisition. The dataset was acquired for two minutes to track the movement of the algae. The resulting SPC-FLIM maps were arranged in Visualization 3, Visualization 4 and Visualization 5. By observing the sample along the measurements, it is possible to identify in the FOV some still algae, which are probably those that have settled on the microscope slide, while others swim regularly. We show in the lower row of Fig. 4 three selected SPC-FLIM maps from Visualization 3 after (a) 2.75 s, (b) 3.85 s and (c) 5.30 s, while the upper row of Fig. 4 shows the high-resolution intensity images acquired by the CMOS camera.

From these FLIM maps, we selected three different algae and monitored their fluorescence lifetime values throughout the entire acquisition. A selected pixel in correspondence to one still alga in Visualization 3 (which can also be located with the red arrow in Fig. 4(a), lower row) shows the lifetimes reported in Fig. 5(a). The lifetime is 2.08 ± 0.04 ns for the initial 180 frames (9 seconds). This lifetime is close to that of the longest component retrieved from a multiexponential fit of TCSPC in bulk algal suspension [27,28], under conditions where photochemical reactions leading to the reduction of photosystem acceptors do not take place [29–33]. The longest lifetime would dominate the average lifetime value retrieved in FLIM data, indicating that the measuring

Optics EXPRESS

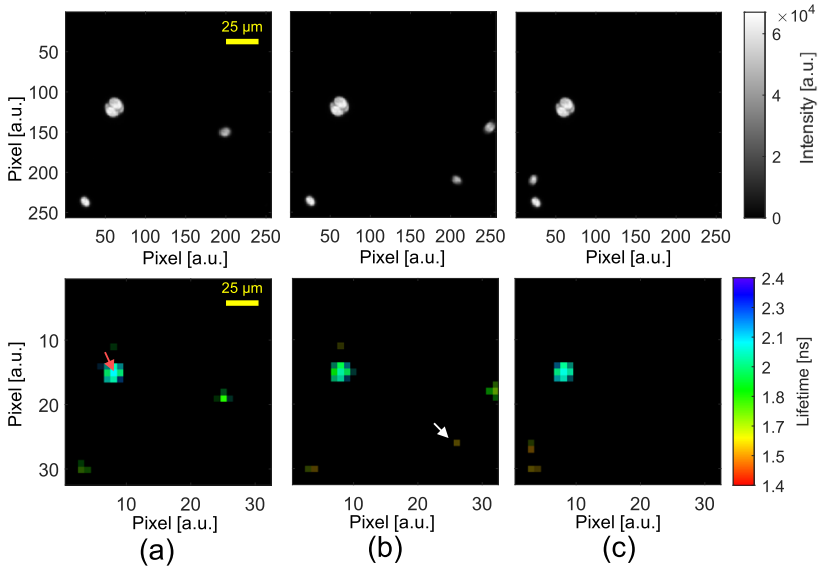

Fig. 4. Measurements with free moving *C. reinhardtii* algae sample at different time instants after the start of the acquisition. Upper row: reference intensity images with a high-resolution CMOS camera. Lower row: FLIM maps acquired with a CS-SPC. (a) after 2.75 s (b) after 3.85 s (c) after 5.30 s.

light is sufficiently intense to maintain the photosystems in the close, photochemically inactive, state. After the first 9 second of acquisition, the lifetime time dependence shows a typical quenching profile, that can be interpreted as the onset of non-photochemical quenching process [33], when the cells is subjected to prolonged illumination by light intensity that saturates the photosynthetic electron transport capacity.

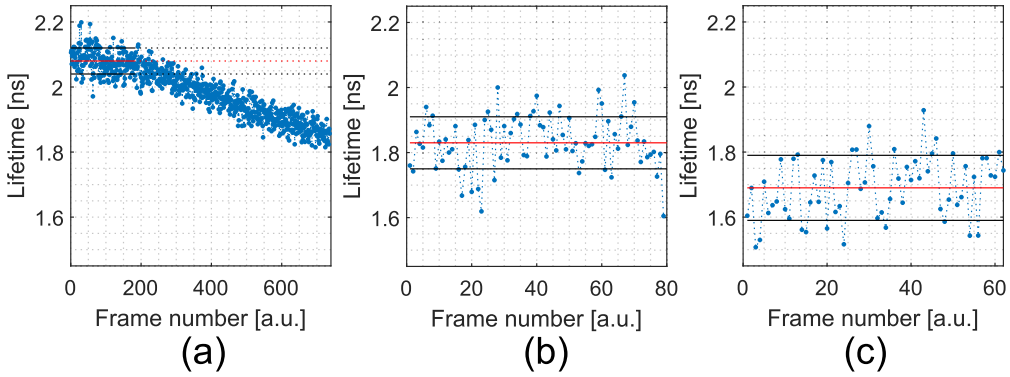

Fig. 5. Lifetime values extracted from three different pixels in the FLIM maps acquired with the *C. reinhardtii* sample across different frames: (a) from the pixel indicated with the red arrow in Fig. 4(a), (b) the moving alga in the first 4 s of Visualization 3, and (c) the moving alga indicated with the white arrow in Fig. 4(b). We show the average of the estimated lifetimes with red lines and the standard deviation with black lines. In (a), the red and black lines refer to the static situation only.

In Fig. 5(b) we present the lifetime of a swimming alga, identifiable within the first 4 seconds of Visualization 3, measuring 1.83 ± 0.08 ns. As for the beads dataset, this value represents the

Optics EXPRESS

estimated lifetime for the pixel containing the alga across different frames. The lifetime maintains a constant profile because the time the alga remains under illumination is not sufficient to cause a significant saturating effect, as it was also found for the first frames of Fig. 5(a). Similarly, the lifetime of another swimming alga, identifiable between ≈3 and ≈5 seconds of Visualization 3 (or in Fig. 4(b) lower row, indicated with white arrow), is 1.69 ± 0.10 ns and exhibits a constant profile over time. The results in Fig. 4 and Fig. 5 demonstrate the capability of the system to resolve multiple lifetimes present in a single image. Similar results are shown in Visualization 4 and 5. Regarding the imaging part, the PSNR across different frames is 28.9 ± 2.4 dB.

In this work the acquisition of high-resolution reference images from the CMOS camera allowed us to evaluate the image quality of the analysed system. In the future, these reference images can be exploited for selecting a ROI within a wider FOV (as a zoom feature), for tracking the sample movement in a smaller area with higher spatial detail. They can also be used for applying data fusion algorithms [16] to enhance the spatial resolution of the SPC-FLIM maps. The parallel acquisition with two detectors required us to halve the fluorescence signal between the CMOS camera and the SiPM. In this case, the 50/50 splitting ratio was adequate for obtaining a count rate close to the limit for the pile-up correction algorithm, but, in general, it can be adjusted for the benefit of the point detector, such as in the case of faint signals or for operating at higher count rates. The latter possibility can be indeed exploited by considering advanced algorithms for pile-up correction for count rates exceeding the asymptotic limit of the laser's repetition rate [34]. In fact, the high count rate limit, the robustness, the excellent timing performance and the wide detection area (which is fundamental for high harvesting efficiency) make SiPMs promising detectors for increasing the SNR and/or the reducing the measurement time. Regarding the measurement process, the proposed system allows us to adjust the projection time for each pattern and hence increase the SNR when a video rate is not required. At the same time, higher compression ratios can be exploited to reduce the measurement time, according to the specific FOV.

4. Conclusions

In this work, we present a high throughput FLIM system designed for studying fast processes such as biological mechanisms in living organisms. We applied this system to track a moving sample and to estimate the lifetime in each pixel of the image with a frame rate of 20 fps. For this purpose, we developed a microscope based on computational imaging and specifically on the compressive single-pixel camera. On the one hand, this was exploited to reduce the number of measurements (CR = 75%) with respect to a conventional scanning scheme and, on the other hand, it allowed us to employ a novel and efficient SiPM detector, coupled to a low dead time TCSPC electronics to work at high photon rates. The proposed system integrates the strength of novel hardware and of a computational approach (compressive sensing, SPC, pile-up correction algorithms). The results we achieved are very promising for biological studies *in vivo*. The SiPM we used is a single-channel detector, but in future it can be scaled into arrays [35] paving the way for multidimensional acquisition. For example, it can provide access to the spectral behavior of the sample, complementing the lifetime information and strengthening specificity for many different applications.

Funding. Ministero dell'Istruzione e del Merito (2020WMSNBL, 2022NEJZ2C); European Commission (CUP B53C22001750006, ID D2B8D520, IR0000016).

Disclosures. The authors declare no conflicts of interest.

Data availability. Data underlying the results presented in this paper are not publicly available at this time but may be obtained from the authors upon reasonable request.

Optics EXPRESS

References

1. R. Datta, T. M. Heaster, J. T. Sharick, *et al.*, "Fluorescence lifetime imaging microscopy: fundamentals and advances in instrumentation, analysis, and applications," J. Biomed. Opt. **25**(07), 1 (2020).
2. C. Stringari, A. Cinquin, O. Cinquin, *et al.*, "Phasor approach to fluorescence lifetime microscopy distinguishes different metabolic states of germ cells in a live tissue," Proc. Natl. Acad. Sci. **108**(33), 13582–13587 (2011).
3. M. Popleteeva, K. T. Haas, D. Stoppa, *et al.*, "Fast and simple spectral FLIM for biochemical and medical imaging," Opt. Express **23**(18), 23511–23525 (2015).
4. J. E. Sorrells, R. R. Iyer, L. Yang, *et al.*, "Single-photon peak event detection (SPEED): a computational method for fast photon counting in fluorescence lifetime imaging microscopy," Opt. Express **29**(23), 37759–37775 (2021).
5. M. Köllner and J. Wolfrum, "How many photons are necessary for fluorescence-lifetime measurements?" Chem. Phys. Lett. **200**(1-2), 199–204 (1992).
6. D. Tyndall, B. R. Rae, D. D.-U. Li, *et al.*, "A high-throughput time-resolved mini-silicon photomultiplier with embedded fluorescence lifetime estimation in 0.13 µm CMOS," IEEE Trans. Biomed. Circuits Syst. **6**(6), 562–570 (2012).
7. A. Cominelli, G. Acconcia, P. Peronio, *et al.*, "High-speed and low-distortion solution for time-correlated single photon counting measurements: A theoretical analysis," Rev. Sci. Instrum. **88**(12), 123701 (2017).
8. X. Liu, D. Lin, W. Becker, *et al.*, "Fast fluorescence lifetime imaging techniques: A review on challenge and development," J. Innov. Opt. Health Sci. **12**(05), 1930003 (2019).
9. W. Yan, X. Peng, J. Qi, *et al.*, "Dynamic fluorescence lifetime imaging based on acousto-optic deflectors," J. Biomed. Opt **19**(11), 116004 (2014).
10. S. P. Poland, N. Krstajić, J. Monypenny, *et al.*, "A high speed multifocal multiphoton fluorescence lifetime imaging microscope for live-cell FRET imaging," Biomed. Opt. Express **6**(2), 277 (2015).
11. R. K. Henderson, N. Johnston, F. Mattioli Della Rocca, *et al.*, "A 192 × 128 Time correlated SPAD image sensor in 40-nm CMOS technology," IEEE J. Solid-State Circuits **54**(7), 1907–1916 (2019).
12. N. Krstajić, S. Poland, J. Levitt, *et al.*, "0.5 billion events per second time correlated single photon counting using CMOS SPAD arrays," Opt. Lett. **40**(18), 4305–4308 (2015).
13. E. J. Candes and M. B. Wakin, "An introduction to compressive sampling," IEEE Signal Process. Mag **25**(2), 21–30 (2008).
14. C. F. Higham, R. Murray-Smith, M. J. Padgett, *et al.*, "Deep learning for real-time single-pixel video," Sci. Rep. **8**(1), 2369 (2018).
15. Y. Ma, Y. Lee, C. Best-Popescu, *et al.*, "High-speed compressed-sensing fluorescence lifetime imaging microscopy of live cells," Proc. Natl. Acad. Sci. **118**(3), e2004176118 (2021).
16. A. Ghezzi, A. J. M. Lenz, F. Soldevila, *et al.*, "Computational based time-resolved multispectral fluorescence microscopy," APL Photonics **8**(4), 046110 (2023).
17. M. P. Edgar, G. M. Gibson, and M. J. Padgett, "Principles and prospects for single-pixel imaging," Nat. Photonics **13**(1), 13–20 (2019).
18. L. Dai, J. Liu, K. Liang, *et al.*, "Realization of a time-correlated photon counting technique for fluorescence analysis," Biomed. Opt. Express **11**(4), 2205–2212 (2020).
19. A. Dalla Mora, L. Di Sieno, A. Behera, *et al.*, "The SiPM revolution in time-domain diffuse optics," Nucl. Instrum. Methods Phys. Res., Sect. A **978**, 164411 (2020).
20. E. Martinenghi, L. Di Sieno, D. Contini, *et al.*, "Time-resolved single-photon detection module based on silicon photomultiplier: A novel building block for time-correlated measurement systems," Rev. Sci. Instrum. **87**(7), 073101 (2016).
21. "https://github.com/andreafarina/CS-FLIM.git," (2024).
22. P. B. Coates, "The correction for photon "pile-up" in the measurement of radiative lifetimes," J. Phys. E: Sci. Instrum. **1**(8), 437878 (1968).
23. E. Avanzi, A. Behera, D. Contini, *et al.*, "Effects and correctability of pile-up distortion using established figures of merit in time-domain diffuse optics at extreme photon rates," Sci. Rep. **12**(1), 5417 (2022).
24. C. Li, W. Yin, H. Jiang, *et al.*, "An efficient augmented Lagrangian method with applications to total variation minimization," Computational Optimization and Applications **56**(3), 507–530 (2013).
25. E. H. Harris, D. B. Stern, and G. B. Witman, *The Chlamydomonas Sourcebook*, 2nd ed. (Academic Press, 2009).
26. S. D. Gallaher, S. T. Fitz-Gibbon, A. G. Glaesener, *et al.*, "Chlamydomonas genome resource for laboratory strains reveals a mosaic of sequence variation, identifies true strain histories, and enables strain-specific studies," The Plant Cell **27**(9), 2335–2352 (2015).
27. A. R. Holzwarth, J. Wendler, and W. Haehnel, "Time-resolved picosecond fluorescence spectra of the antenna chlorophylls in *Chlorella vulgaris*. resolution of photosystem I fluorescence," Biochim. Biophys. Acta, Bioenerg. **807**(2), 155–167 (1985).
28. M. Hodges and I. Mova, "Time-resolved chlorophyll fluorescence studies on photosynthetic mutants of *Chlamydomonas reinhardtii:* origin of the kinetic decay components," Photosynth. Res. **13**(2), 125–141 (1987).
29. W. L. Butler, "Energy distribution in the photochemical apparatus of photosynthesis," Annu. Rev. Plant. Physiol. **29**(1), 345–378 (1978).
30. L. N. M. Duysens, "Transfer and Trapping of Excitation Energy in Photosystem II," in *Ciba Foundation Symposium 61 - Chlorophyll Organization and Energy Transfer in Photosynthesis* (John Wiley & Sons, Ltd, 1979), pp. 323–364.

Optics EXPRESS

31. N. R. Baker, "Chlorophyll fluorescence: a probe of photosynthesis in vivo," Annu. Rev. Plant Biol. **59**(1), 89–113 (2008).
32. P. Horton, A. V. Ruban, and R. G. Walters, "Regulation of light harvesting in green plants," Annu. Rev. Plant Physiol. Plant Mol. Biol. **47**(1), 655–684 (1996).
33. K. Amarnath, J. Zaks, S. D. Park, *et al.*, "Fluorescence lifetime snapshots reveal two rapidly reversible mechanisms of photoprotection in live cells of Chlamydomonas reinhardtii," Proc. Natl. Acad. Sci. U.S.A. **109**(22), 8405–8410 (2012).
34. S. Isbaner, N. Karedla, D. Ruhlandt, *et al.*, "Dead-time correction of fluorescence lifetime measurements and fluorescence lifetime imaging," Opt. Express **24**(9), 9429–9445 (2016).
35. E. Avanzi, A. Ghezzi, A. Farina, *et al.*, "Evaluation of the timing performance of silicon photomultiplier detectors array and its preliminary application in fluorescence lifetime sensing and diffuse optics," in *Optical Tomography and Spectroscopy of Tissue XV*, S. Fantini and P. Taroni, eds. (SPIE, 2023), p. 47.